AIP | Applied Physics Letters

Laboratory-based X-ray phase-contrast imaging with misaligned optical elements

Marco Endrizzi, Dario Basta, and Alessandro Olivo

Citation: Applied Physics Letters **107**, 124103 (2015); doi: 10.1063/1.4931778
View online: http://dx.doi.org/10.1063/1.4931778
View Table of Contents: http://scitation.aip.org/content/aip/journal/apl/107/12?ver=pdfcov
Published by the AIP Publishing

Articles you may be interested in

Quantitative electron density characterization of soft tissue substitute plastic materials using grating-based x-ray phase-contrast imaging
Rev. Sci. Instrum. **85**, 103708 (2014); 10.1063/1.4898052

Noise in x-ray grating-based phase-contrast imaging
Med. Phys. **38**, 4133 (2011); 10.1118/1.3592935

Large-Area Phase-Contrast X-ray Imaging System Based on a Two-Crystal X-ray Interferometer
AIP Conf. Proc. **716**, 22 (2004); 10.1063/1.1796575

Large-Area Phase-Contrast X-ray Imaging System Using a Two-Crystal X-ray Interferometer—Development of an Interference-Pattern-Based Feedback Positioning System
AIP Conf. Proc. **705**, 1299 (2004); 10.1063/1.1758039

Phase-contrast hard x-ray imaging microscope with Wolter mirror optics
AIP Conf. Proc. **507**, 84 (2000); 10.1063/1.1291123

This article is copyrighted as indicated in the article. Reuse of AIP content is subject to the terms at: http://scitation.aip.org/termsconditions. Downloaded to IP: 128.41.35.96 On: Tue, 15 Dec 2015 15:11:14

Laboratory-based X-ray phase-contrast imaging with misaligned optical elements

Marco Endrizzi, Dario Basta, and Alessandro Olivo
Department of Medical Physics and Biomedical Engineering, University College London, Gower Street, WC1E 6BT London, United Kingdom

(Received 14 July 2015; accepted 15 September 2015; published online 24 September 2015)

We report on a laboratory X-ray phase-contrast imaging technique based on the edge illumination principle that substantially relaxes the existing limitations on system set up and data acquisition, allowing an increase in tolerance of misalignments by at least two orders of magnitude. The robustness of this approach was systematically studied by means of experiments with our prototype. Numerical simulations were also performed in order to assess the dependence of the image quality on the data acquisition scheme. The results show that errors in the positioning of the masks within a 1° range for all the angles, and within 1 mm range of translation, do not noticeably affect image quality. We also show that, if the misalignment does not exceed few tens of micrometers, three intensity projections are sufficient to effectively retrieve the three representations of the sample, allowing for optimization of dose or time efficiency even with a non-ideal system. © *2015 AIP Publishing LLC*. [http://dx.doi.org/10.1063/1.4931778]

X-ray phase-contrast imaging (XPCI) extends the potential of conventional radiography by introducing sensitivity also to the phase-shifts imparted to the X-ray beam when it passes through the sample,[1,2] finding application in areas as diverse as medicine, materials engineering, security screening, and quality control in industry. While several approaches have been developed to perform XPCI,[3] one of the major challenges that still remains open is that of making the potential of these methods widely available through the development of techniques that are fast, robust, and reliable.

Edge illumination (EI)[4,5] is a non-interferometric XPCI technique enabling the quantitative retrieval of absorption, refraction and ultra-small-angle scattering in the sample, also under weak partial coherence.[6–8] The coherence length is typically around 0.5 μm, much smaller than the characteristics lengths of the optical masks. The energy distribution is usually broad, with an energy spread of $\Delta E/\bar{E} = 0.3 - 0.7$. EI was proven to provide high sensitivity, at synchrotrons as well as in laboratory-scale implementations,[9–11] to efficiently use the entire spectrum produced by conventional X-ray tubes[12] and to be suitable for quantitative three-dimensional imaging.[13,14]

Here, we propose a laboratory-based approach for multimodal XPCI, which uses a conventional rotating anode X-ray source, two partially absorbing optical elements, and a flat panel sensor. The basic mechanism for generating contrast is that of EI; however, the model, data acquisition, and processing algorithm have been specifically designed to relax the requirements on the alignment[15] by more than two orders of magnitude. This offers the possibility to overcome the limitations related to inaccuracies in the spatial positioning of the optical elements. Moreover, it also corrects for the possible errors due the precision and uniformity with which optical masks, covering several square centimetres of field of view, can be manufactured. The approach was experimentally tested on a custom built phantom, which was imaged while gradually degrading the accuracy of the system's alignment, without this affecting the resolution or the quality of the images. A set of numerical simulations was also performed in order to assess within which limits it is possible to minimize the number of intensity projections and therefore optimize the dose delivered to the sample.

The typical set-up for an EI experiment is composed of an X-ray source, a mask that shapes the radiation before it reaches the sample, and another mask that serves as an analyser, and it is placed just in front of the detector. When an X-ray tube with an extended source is used, the very weak coherence conditions allow for a geometrical optics description of the image formation. When one mask is translated by a length x with respect to the other, the measured intensity is given by:[7]

$$\frac{I(x)}{I_0} = (L * O)(x - \Delta x_R)t, \tag{1}$$

where I_0 is the intensity transmitted by the sample aperture, L is the illumination function that describes how the intensity detected changes depending upon the relative position of the two masks, O is the scattering distribution induced by the sample, Δx_R is the shift imparted to the beam by refraction, t is the fraction of intensity transmitted through the sample, and * indicates convolution. This convolution equation can be written in the following form:[7]

$$\frac{I(x)}{I_0} = t\sum_m \sum_n A_{mn} \exp\left[-\frac{(x-\mu_{mn})^2}{2\sigma_{mn}^2}\right], \tag{2}$$

where $L(x) = \sum_n (A_n/\sqrt{2\pi\sigma_n^2}) \exp[-(x-\mu_n)^2/2\sigma_n^2]$ and the index n runs between $n=1$ and $n=N$; and $O(x) = \sum_m (A_m/\sqrt{2\pi\sigma_m^2}) \exp[-(x-\mu_m)^2/2\sigma_m^2]$, and the index m runs between $m=1$ and $m=M$. The parameters are defined as follows: $\mu_{mn} = \mu_m + \mu_n$, $\sigma_{mn}^2 = \sigma_m^2 + \sigma_n^2$, and $A_{mn} = A_m A_n (1/\sqrt{2\pi\sigma_{mn}^2})$. This provides an analytical function that can be used to numerically retrieve the unknown parameters, i.e.,

 © 2015 AIP Publishing LLC

This article is copyrighted as indicated in the article. Reuse of AIP content is subject to the terms at: http://scitation.aip.org/termsconditions. Downloaded to IP: 128.41.35.96 On: Tue, 15 Dec 2015 15:11:14

the properties of the imaged sample. This retrieval approach, as opposed to that of analytically inverting a simplified version of Eq. (2),[7] offers several advantages. It can be used with basically any EI system, the specific parameters of which (mask aperture, pitch, material, thickness, source size and shape, etc.) can be unknown. The masks can be non-ideal, e.g., they can be partially transmitting or imperfectly regular. The illumination function can be measured experimentally, and this provides a complete characterization of the imaging system, sufficient to perform the retrieval. The number of points and the positions at which Eq. (2) is sampled are arbitrary, offering more flexibility from both the experimental and the optimization point of view. This option to choose points arbitrarily, together with the observation that Eq. (2) holds on a pixel-by-pixel basis, enables a significant relaxation of the requirements on system alignment. This accounts for unavoidable inaccuracies such as the precision with which the optical elements can be fabricated or the fact that we are analysing a spherical wavefront with a flat mask. In addition, it takes into account also errors coming from sources such as thermal drifts or actual mask misalignment.

For this experiment, the scattering distribution O is assumed to be a Gaussian ($M = 1$) while no assumptions are made on the illumination function L, and we empirically found that two terms ($N = 2$) are sufficient to accurately describe it. The illumination function L_{ij} is measured independently for each detector pixel (i, j) without sample first. The properties of the sample are then retrieved by using the known form of L_{ij} and looking at the changes in terms of integrated area (attenuation), centre shift (refraction), and broadening (ultra-small-angle scattering). We implemented this by solving a non-linear curve-fitting problem, in the least-squares sense $\min_b \sum_p [G(b, x_p) - I_p]^2$, where G is the model function, b its set of parameters, and I_p are the X-ray intensities measured at different illumination positions x_p, with $p = 1 \ldots P$. In other words, we searched for the set of parameters b that minimises the squared difference between the data and the model function. The total area A, centre position μ, and width σ of the intensity distribution were initially estimated directly from the data as $A = \sum I_p$, $\mu = \sum I_p x_p / \sum I_p$, and $\sigma^2 = \sum I_p (x_p - \mu)^2 / \sum I_p$, respectively, and these values were used as the initial guess for the fitting procedure.

In order to demonstrate the robustness of the proposed approach, we performed several scans by deliberately misaligning the sample mask. With respect to the aligned position, we moved the sample mask around all angles in a 1° range [−0.5°, +0.5°] and along the z axis in a 1 mm range [−500 μm, +500 μm] (see Fig. 1). These four degrees of freedom have been altered one at a time first, then in combination. The retrieved images are then compared in terms of signal and noise. These have been defined in the following way, for the different types of contrast obtained with the technique. For attenuation images, the signal is taken as $S_a = (I_{det} - I_{bkg})/I_{bkg}$, where I_{det} indicates the intensity measured over a detail of interest and I_{bkg} the intensity in the background. The noise is measured as the sum in quadrature of the standard deviations of these two quantities

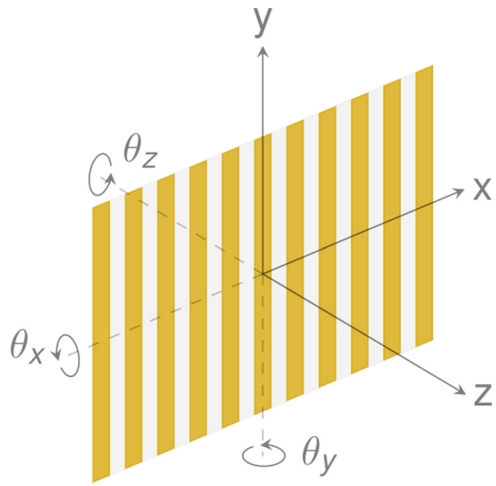

FIG. 1. Sketch of the degrees of freedom for the pre-sample mask. The beam propagates along the z axis, the apertures extend along y, and the system is sensitive to refraction only along the x direction.

$N_a = \sqrt{\sigma_{det}^2 + \sigma_{bkg}^2}$. For refraction images, the signal is taken as the difference between the bright and the dark fringes occurring at the edge of the detail $S_r = \max(R) - \min(R)$, where R is the refraction angle. The noise is evaluated as the standard deviation of the background $N_r = \sigma_R$. For dark-field images, the signal is given by the value of the standard deviation of the scattering distribution $S_d = \sigma_M$. The noise is described as the signal fluctuations in a background region $N_d = \sigma_{S_d}$.

The test sample consists of a perspex tube, with diameter 2 cm and wall thickness 2 mm, containing a perspex cylinder of 3 mm diameter and an expanded polystyrene "peanut" commonly used for packing fragile objects. In order to acquire several intensity projections at different points along the illumination function, the images were acquired by shifting the sample mask over 7 positions ($P = 7$), equally spaced within the mask's pitch (10 μm steps). Dithering[5] was used to avoid aliasing and improve the spatial resolution: the sample was scanned in 7 sub-pixel steps of 11.3 μm.

The influence of the number of intensity projections P is investigated by means of simulations. A numerical sample is generated by random extraction of three 100×100 matrices from the intervals: [0.5, 1] for transmission, [0, 2] μrad for refraction, and [0, 8] μrad for scattering. For every number of projections P considered, we simulated that these were acquired at evenly spaced positions, with a relative distance of $q_1/(P + 1)$ from one another. The detector is simulated as an ideal photon counter, and the noise is added according to Poisson's statistics. For this set of simulations, the number of photons going through the sample aperture is kept constant at 10^4, and this number is divided among the projections P, by assuming a constant integration time for the detector at each position. In a practical situation, this corresponds to keeping constant the total acquisition time and the dose delivered to the sample. The misalignment of the sample mask is simulated by means of a random process. For each pixel, the relative shift of the illumination function centre is randomly extracted from a uniform distribution. This was

This article is copyrighted as indicated in the article. Reuse of AIP content is subject to the terms at: http://scitation.aip.org/termsconditions. Downloaded to IP: 128.41.35.96 On: Tue, 15 Dec 2015 15:11:14

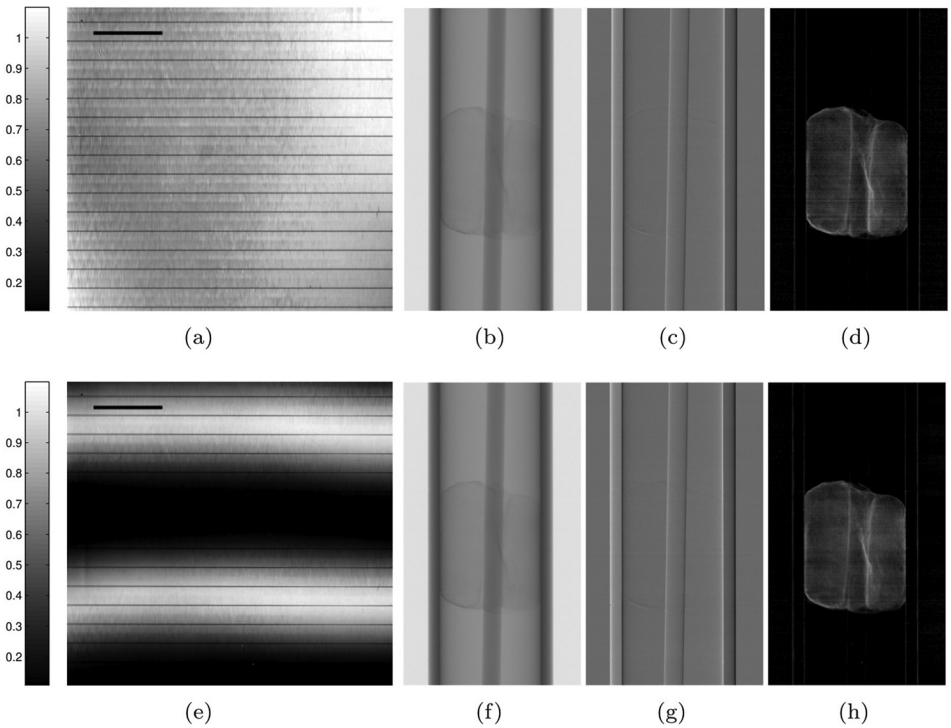

FIG. 2. Visual comparison between the images obtained with the system aligned in panels (b)–(d), and misaligned in panels (f)–(h), for the transmission, refraction, and scattering images. Although the illumination is extremely different in the two cases, as it can be seen by comparing panels (a) and (e), the retrieved images are very similar one to each other. For panels (a)–(d), the system is aligned to within 2 μm while in the (e)–(h) cases the total misalignment is larger than 80 μm. The scale bar is 1 cm.

found to be a good representation of the real experimental conditions. Three different cases were considered: $W = 2$, $W = 20$, and $W = 60\,\mu$m width, which can be, respectively, considered as small, mild, and severe misalignment. The actual values for the masks' specification, system geometry, detector, and source characteristics were the same used for the experiment, described in the following.

The EI imaging system features a sample mask of pitch $q_1 = 79\,\mu$m and aperture $r_1 = 23\,\mu$m, a detector mask with pitch $q_2 = 98\,\mu$m and aperture $r_2 = 29\,\mu$m and a detector pixel pitch $q_3 = 50\,\mu$m. The source size is 70 μm, and the sample mask is at 1.6 m from the source while the detector mask is placed a further 0.4 m downstream. The source is a rotating anode molybdenum target and was operated at 40kv/25 mA (Rigaku, MM007), and the detector is a CMOS image sensor (Hamamatsu, C9732DK-11) and was used with a line-skipping[16] mask design.

A visual comparison of images obtained with a misaligned EI system, against those acquired with an aligned one, is presented in Fig. 2. Panels 2(a) and 2(e) show the illumination across about $5 \times 5\,\text{cm}^2$ field of view. It is apparent that, in the misaligned case, the illumination is highly nonuniform while it is approximately flat in the aligned case. In case 2(e), the sample mask was misaligned by displacing a combination of degrees of freedom: θ_x by $-0.1°$, θ_y by $0.1°$, θ_z by $0.2°$, and z by -0.1 mm; for a combined misalignment exceeding one pitch of the sample mask. The attenuation and refraction signals were measured for the plastic cylinder while the polystyrene was used to measure scattering. Their values, extracted from a range of images acquired with different misalignment of each degree of freedom, are summarised in Fig. 3. The performance of the imaging system appears to be consistent across all the situation investigated, with the attenuation and refraction signals fluctuating by only few percent. The scattering signal fluctuates more strongly, around about 20%; however, it does not show any detectable trend while the sample mask is progressively misaligned. Noise levels were measured at 0.0026, 0.16 μrad,

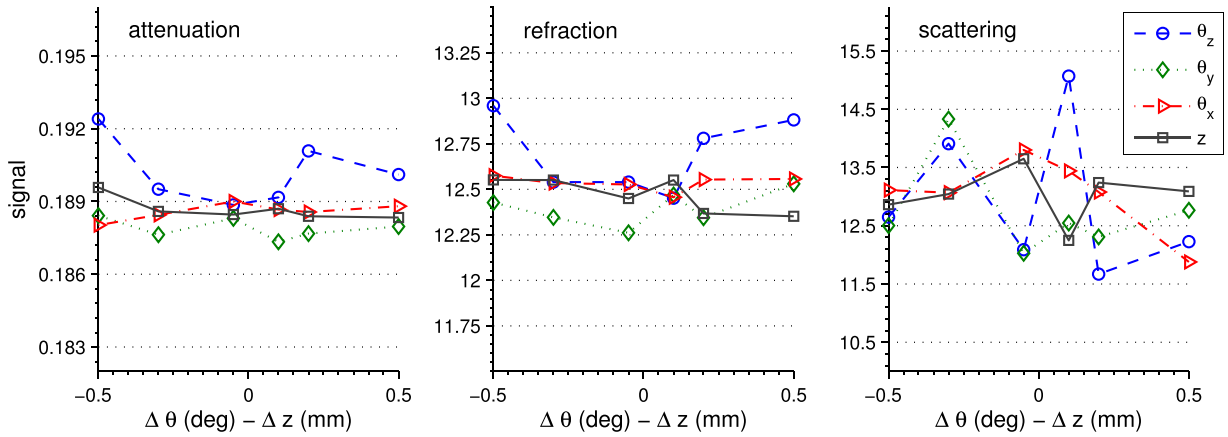

FIG. 3. Attenuation, refraction, and scattering signals plotted against several misaligned positions, for the four degrees of freedom θz, θy, θx, and z. No clear trend can be identified as a function of misalignment across all contrast channels.

This article is copyrighted as indicated in the article. Reuse of AIP content is subject to the terms at: http://scitation.aip.org/termsconditions. Downloaded to IP: 128.41.35.96 On: Tue, 15 Dec 2015 15:11:14

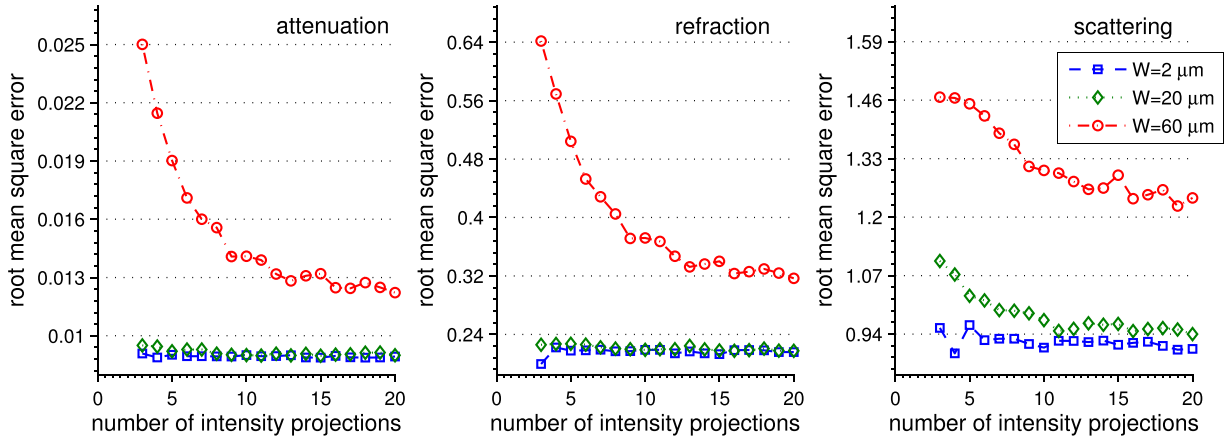

FIG. 4. Numerical simulation results for the optimization of the number of acquired intensity projections. A large number of images at various illumination levels is crucial only when the system is strongly misaligned ($W = 60\,\mu$m). A small number of intensity projections are sufficient when the overall misalignment of the system is smaller than the pitch of the sample mask.

and 1.4 μrad for the attenuation, refraction, and scattering images, respectively. The observation that the refraction image signal is not reduced indicates that also the spatial resolution is preserved, even with the system completely out of alignment. The signal is measured on a sharp feature such as the edge of the cylinder, and a degradation of the spatial resolution would result in a decreased maximum intensity of the measured peaks. Since this decrement is not observed, we can exclude the possibility that a misaligned system leads to images with degraded spatial resolution.

The results of the numerical simulations investigating how the sampling along the illumination function affects the results in various misalignment conditions are reported in Fig. 4. A large number of intensity projections become important only when the misalignment of the imaging system is large, i.e., it becomes comparable to or larger than the pitch of the sample mask. When the system is moderately out of alignment (less than 20 μm across the field of view), three points are sufficient to retrieve the transmission, refraction, and scattering images. Scattering exhibits a slight degradation, in the $W = 20\,\mu$m case, in the acquisitions with fewer projections. This degradation is small; however, it indicates that scattering is the most sensitive amongst the retrieved quantities. Besides making the data acquisition procedure simpler, the collection of fewer points is advantageous in terms of dose delivery and time efficiency consideration.

We proposed an approach to multi-modal X-ray phase-contrast imaging which enables the effective retrieval of attenuation, phase, and dark-field images also with misaligned and/or defective optical elements. Sources of error which are simultaneously taken into account include both optical elements imperfections, due to the limits affecting the manufacturing process, and positioning inaccuracies such as motor errors and thermal drifts. All these sources of error are accounted for in the retrieval, resulting in an extremely robust X-ray phase-contrast imaging method, which is compatible with laboratory instrumentation. This was experimentally demonstrated over a range of 1° for all the angles involved in the alignment of the optical elements, as well as for a range of 1 mm of linear translation along the X-ray beam axis. In addition, numerical simulations showed that, for misalignment ranges of few tens of micrometres, three projections are still sufficient to correctly retrieve the three multi-modal images of the sample, therefore enabling dose optimization also when non-optimized imaging systems are used.

This work was supported by the UK Engineering and Physical Sciences Research Council Grant EP/I021884/1 and Science and Technology Facilities Council Grant ST/L502662/1. M.E. was supported by a Marie Curie Career Integration Grant, No. PCIG12-GA-2012-334056, within the Seventh Framework Programme of the European Union.

[1]R. Fitzgerald, "Phase-sensitive x-ray imaging," Phys. Today **53**(7), 23–26 (2000).
[2]A. Bravin, P. Coan, and P. Suortti, "X-ray phase-contrast imaging: From pre-clinical applications towards clinics," Phys. Med. Biol. **58**(1), R1 (2013).
[3]S. W. Wilkins, Y. I. Nesterets, T. E. Gureyev, S. C. Mayo, A. Pogany, and A. W. Stevenson, "On the evolution and relative merits of hard x-ray phase-contrast imaging methods," Philos. Trans. R. Soc., A **372**, 20130021 (2014).
[4]A. Olivo, F. Arfelli, G. Cantatore, R. Longo, R. H. Menk, S. Pani, M. Prest, P. Poropat, L. Rigon, G. Tromba, E. Vallazza, and E. Castelli, "An innovative digital imaging set-up allowing a low-dose approach to phase contrast applications in the medical field," Med. Phys. **28**, 1610–1619 (2001).
[5]A. Olivo and R. Speller, "A coded-aperture technique allowing x-ray phase contrast imaging with conventional sources," Appl. Phys. Lett. **91**(7), 074106 (2007).
[6]P. R. Munro, K. Ignatyev, R. D. Speller, and A. Olivo, "Phase and absorption retrieval using incoherent x-ray sources," Proc. Natl. Acad. Sci. U.S.A. **109**(35), 13922–13927 (2012).
[7]M. Endrizzi, P. C. Diemoz, T. P. Millard, J. L. Jones, R. D. Speller, I. K. Robinson, and A. Olivo, "Hard x-ray dark-field imaging with incoherent sample illumination," Appl. Phys. Lett. **104**(2), 024106 (2014).
[8]M. Endrizzi and A. Olivo, "Absorption, refraction and scattering retrieval with an edge-illumination-based imaging setup," J. Phys. D: Appl. Phys. **47**(50), 505102 (2014).
[9]P. C. Diemoz, M. Endrizzi, C. E. Zapata, Z. D. Pešić, C. Rau, A. Bravin, I. K. Robinson, and A. Olivo, "X-ray phase-contrast imaging with nanoradian angular resolution," Phys. Rev. Lett. **110**, 138105 (2013).
[10]P. C. Diemoz, C. K. Hagen, M. Endrizzi, and A. Olivo, "Sensitivity of laboratory based implementations of edge illumination x-ray phase-contrast imaging," Appl. Phys. Lett. **103**(24), 244104 (2013).
[11]M. Endrizzi, F. A. Vittoria, P. C. Diemoz, R. Lorenzo, R. D. Speller, U. H. Wagner, C. Rau, I. K. Robinson, and A. Olivo, "Phase-contrast

This article is copyrighted as indicated in the article. Reuse of AIP content is subject to the terms at: http://scitation.aip.org/termsconditions. Downloaded to IP: 128.41.35.96 On: Tue, 15 Dec 2015 15:11:14

microscopy at high x-ray energy with a laboratory setup," Opt. Lett. **39**(11), 3332–3335 (2014).
[12]M. Endrizzi, F. A. Vittoria, G. Kallon, D. Basta, P. C. Diemoz, A. Vincenzi, P. Delogu, R. Bellazzini, and A. Olivo, "Achromatic approach to phase-based multi-modal imaging with conventional x-ray sources," Opt. Express **23**(12), 16473–16480 (2015).
[13]C. K. Hagen, P. C. Diemoz, M. Endrizzi, L. Rigon, D. Dreossi, F. Arfelli, F. C. M. Lopez, R. Longo, and A. Olivo, "Theory and preliminary experimental verification of quantitative edge illumination x-ray phase contrast tomography," Opt. Express **22**(7), 7989–8000 (2014).
[14]C. K. Hagen, P. R. T. Munro, M. Endrizzi, P. C. Diemoz, and A. Olivo, "Low-dose phase contrast tomography with conventional x-ray sources," Med. Phys. **41**(7), 070701 (2014).
[15]T. P. Millard, M. Endrizzi, K. Ignatyev, C. K. Hagen, P. R. T. Munro, R. D. Speller, and A. Olivo, "Method for automatization of the alignment of a laboratory based x-ray phase contrast edge illumination system," Rev. Sci. Instrum. **84**(8), 083702 (2013).
[16]K. Ignatyev, P. R. T. Munro, R. D. Speller, and A. Olivo, "Effects of signal diffusion on x-ray phase contrast images," Rev. Sci. Instrum. **82**(7), 073702 (2011).

This article is copyrighted as indicated in the article. Reuse of AIP content is subject to the terms at: http://scitation.aip.org/termsconditions. Downloaded to IP: 128.41.35.96 On: Tue, 15 Dec 2015 15:11:14